Pacific Graphics (2014)
J. Keyser, Y. J. Kim, and P. Wonka (Editors)

Incorporating Fiber Controls into FEM Model for Transversely Isotropic Materials

Cai Jianping[1], Lin Feng[1], Lee Yong Tsui[2], Qian Kemao[1], Seah Hock Soon[1]

[1]School of Computer Engineering, [2]School of Mechanical and Aerospace Engineering
Nanyang Technological University, Singapore

Abstract

Physically plausible deformable models based on continuum mechanics have been a hot topic in computer graphics for decades, and many models have been proposed to improve performance speed and stability. However, most of the existing models focus on isotropic materials, while elastic objects with complex anisotropic properties are less studied. Based on the observation that a large group of objects have specific internal structures (fibers) that determine their anisotropic behavior, we propose a fiber incorporated corotational FEM model that can approximate ***longitudinally*** *anisotropic deformation. First, a fiber orientation field is used to establish local frames for each element; then, the orientation information is combined into the FEM model by adding local transformations on element stiffness matrices. This proposed model can provide a control for directable deformations, and yields realistic anisotropic deformations. Large deformations can be accommodated; meanwhile, with pre-computation it adds no computational cost to the existing corotational FEM model during simulation. Convincing experimental results and analytical comparisons are presented, together with an accompanying video demonstration.*

Categories and Subject Descriptors (according to ACM CCS): I.3.5 [Computer Graphics]: Computational Geometry and Object Modeling—Physically based modeling

1. Introduction

In computer graphics, simulation of deformable objects has been developed for nearly three decades since Terzopoulos et al. [TPBF87] introduced elastically deformable models in the late 1980s. Many papers have been published, and they can be categorized into two approaches: geometrically based deformable models and physically based deformable models.

Geometrically based deformable models are fast and controllable, which well suit interactive applications such as computer games. Typical methods such as shape matching method [MHTG05], position based method [MHHR07] and oriented particles [MC11] can produce visually plausible dynamic deformations. We refer readers to a recent report [BMO*14] for details. However, these models cannot generate physically accurate deformations due to the lack of physics basis.

Physically based methods are defined by continuum mechanics, in which mechanical behaviors are formulated by the constitutive model of the simulated material. Well established methods such as finite difference method, finite volume method, boundary element method and finite element method (FEM) have been adopted in computer graphics, and for a thorough review we refer readers to a survey paper [NMK*06] by Nealen et al. For computation of the continuum model, FEM is proved to be the most suitable numerical method; it can efficiently solve partial differential equations on irregularly discretized grid.

Although physically based models are able to yield physically authentic results, they are much more computationally intensive; and in some cases, the prohibitive execution time prevents their practical applications. To reduce the burden in computation, researchers have made a lot of efforts to improve the stability and speed, such as the corotational linear FEM (CLFEM) [MG04], the invertible FEM [ITF04], the total Lagrangian explicit dynamics method (TLED) [MJLW07] [Com10], and the model reduc-

DOI: 10.2312/pgs.20141243

tion methods [BJ05] [CK05] [KJ12]. However, most of these methods have only been adopted to deal with deformation of isotropic materials.

To simulate complex deformations with anisotropic materials, an example based method [MTGG11] [KTUI12] has been proposed. Several pre-defined deformed poses of an object are required, which control the deformations during dynamic simulation. In [TTL12], virtual muscle fibers are defined for a simple soft body, whose lengths are determinded by locomotion controllers; the fibers are then used to control the locomotion of the body, which is similar to the skeleton-driven deformation. Based on the observation that many real-world objects are composites with a base matrix material and fiber structures, a fiber reinforced model [LHR*12] has been proposed; 1D curves (as the fibers) are interactively embedded into a solid object, and internal forces are computed according to deformation energies of both the solid and curves. These methods can produce impressive deformations, but adds much more computational cost to the existing FEM model. Meanwhile, a recent paper [LBKS14] provides an intuitive and stable way for the user to tune material parameters for orthotropic materials.

In this paper, we propose a fiber incorporated FEM model for anisotropic elastic materials. Especially, we are interested in transversely isotropic materials which are commonly found in fiber constructed objects, such as plant tissues and muscular tissues in animals; thus, in this paper *anisotropic* refers to *longitudinally anisotropic* except the discussions/descriptions of related work and background. The main advantages of our model are:

i. Rather than computing deformation energy of the embedded curves as in the fiber reinforced model, we use the directions of the curves only to define an orientation field.

ii. Instead of one spatial coordinate system, a local frame is established for each element according to the fiber directions; element stiffness matrices and internal forces are computed in these local frames. By coordinate system transformations, we can then assemble all the elements in the global frame to achieve the anisotropic deformation.

iii. A corotational linear FEM model is used, which is faster than nonlinear FEM models; and large deformations can be accommodated.

iv. Additional computations in our model can be done in pre-computation phase, thus no additional computational cost is added to the existing FEM model during simulation.

In the following sections, we first introduce the formulation of the anisotropic elasticity in Section 2. Then, we present our fiber incorporated corotational linear FEM model in Section 3. We show the simulation examples to demonstrate the effectiveness of our model, and give some comparative analysis in Section 4. Convincing real-time animations can be seen in the accompanying video.

2. Formulation of Linear Anisotropic Elasticity

In continuum mechanics, the mechanical behavior of a material is defined by *constitutive equation* (the stress-strain law), which represents the relationship between stress σ and strain ε as $\sigma = \mathbf{C}\varepsilon$, and $\mathbf{C}$ is the elastic stiffness matrix. In the three-dimensional case, it can be written in a *contracted form* [TH96] as

$$\begin{pmatrix} \sigma_x \\ \sigma_y \\ \sigma_z \\ \tau_{xy} \\ \tau_{yz} \\ \tau_{zx} \end{pmatrix} = \begin{pmatrix} C_{11} & C_{12} & C_{13} & C_{14} & C_{15} & C_{16} \\ & C_{22} & C_{23} & C_{24} & C_{25} & C_{26} \\ & & C_{33} & C_{34} & C_{35} & C_{36} \\ & & & C_{44} & C_{45} & C_{46} \\ & sym. & & & C_{55} & C_{56} \\ & & & & & C_{66} \end{pmatrix} \begin{pmatrix} \varepsilon_x \\ \varepsilon_y \\ \varepsilon_z \\ \gamma_{xy} \\ \gamma_{yz} \\ \gamma_{zx} \end{pmatrix}, \quad (1)$$

where $\mathbf{C}$ is a 6×6 symmetric matrix; σ and ε are 6×1 column matrices; $\sigma = (\sigma_x\ \sigma_y\ \sigma_z\ \tau_{xy}\ \tau_{yz}\ \tau_{zx})^{\mathrm{T}}$ and $\varepsilon = (\varepsilon_x\ \varepsilon_y\ \varepsilon_z\ \gamma_{xy}\ \gamma_{yz}\ \gamma_{zx})^{\mathrm{T}}$, where the single-letter subscripted σ and ε are normal stresses and normal strains respectively, and the double-letter subscripted τ and γ are shear stresses and shear strains respectively. Therefore, it can have as many as 21 elastic parameters.

2.1. Transversely Isotropic Material

The number of elastic parameters can be reduced when the material possesses certain material symmetry properties. Isotropic materials are an extreme case which has only two material parameters, and its mechanical response is independent of directions in the material space.

We start with transversely isotropic materials which are commonly seen in real world objects. This kind of materials can be characterized by a symmetry plane and an axis orthogonal to this plane. In our discussions, the material symmetry is defined in a three-dimensional coordinate system $\{\mathbf{x}_1, \mathbf{x}_2, \mathbf{x}_3\}$; for example, the symmetry planes includes the $\mathbf{x}_3 = 0$ and any plane that contains the $\mathbf{x}_3$-axis. Thus, the number of elastic parameters is reduced to *five*, such that

$$\mathbf{C} = \begin{pmatrix} C_{11} & C_{12} & C_{13} & 0 & 0 & 0 \\ & C_{22} & C_{23} & 0 & 0 & 0 \\ & & C_{33} & 0 & 0 & 0 \\ & & & C_{44} & 0 & 0 \\ & sym. & & & C_{55} & 0 \\ & & & & & C_{66} \end{pmatrix}, \quad (2)$$

where $C_{11} = C_{22}, C_{13} = C_{23}, C_{55} = C_{66}, C_{44} = \frac{1}{2}(C_{11} - C_{12})$.

2.2. Continuum Elasticity

Given an elastic body Ω, its deformation can be specified by a displacement field $\mathbf{d} = \mathbf{d}(\mathbf{x})$. That is, a material point $\mathbf{x}$ in the undeformed configuration is deformed to a point $\mathbf{p} = \mathbf{x}+\mathbf{d}$ in the deformed configuration. For small deformations,

the strain ε can be defined by *Cauchy's linear strain tensor*,

$$\varepsilon = \begin{pmatrix} \frac{\partial}{\partial x} & 0 & 0 \\ 0 & \frac{\partial}{\partial y} & 0 \\ 0 & 0 & \frac{\partial}{\partial z} \\ \frac{\partial}{\partial y} & \frac{\partial}{\partial x} & 0 \\ 0 & \frac{\partial}{\partial z} & \frac{\partial}{\partial y} \\ \frac{\partial}{\partial z} & 0 & \frac{\partial}{\partial x} \end{pmatrix} \begin{pmatrix} u \\ v \\ w \end{pmatrix} = \mathbf{L}\mathbf{d}, \quad (3)$$

where $\mathbf{L}$ is the strain operator. The elastic strain energy can then be defined by

$$U = \int_\Omega \frac{1}{2} \varepsilon^{\mathrm{T}} \mathbf{C} \varepsilon \, d\Omega. \quad (4)$$

As for the dynamics of deformation, it is defined by Newton's Second law,

$$m\ddot{\mathbf{d}} + c\dot{\mathbf{d}} + \mathbf{f}_{int} = \mathbf{f}_{ext}, \quad (5)$$

where m is the mass of a material point, $\ddot{\mathbf{d}}$ the acceleration, c the damping coefficient, $\dot{\mathbf{d}}$ the velocity, $\mathbf{f}_{int} = \frac{\partial U}{\partial \mathbf{x}}$ the internal force, and $\mathbf{f}_{ext}$ the external applied force.

Finite element method solves this continuum problem by discretizing the continuous body into a finite amount of small elements, and the mechanical quantities are obtained by interpolation of the values on the nodes using shape functions.

3. Fiber Incorporated FEM Model

3.1. Accomodation of Large Deformation with a Corotational Linear FEM Model

We propose to incorporate a fiber orientation field into the CLFEM model [MG04] that can deal with larger deformations than a linear model. We describe the key formula for implementing the CLFEM in this section; in the next section, we show how to incorporate the fiber orientation information with the CLFEM to simulate the dynamics of anisotropic elastic materials. Note that most of the discussions encompass a single tetrahedron element, in which a quantity is superscripted by 'e'.

In our algorithm, a tetrahedral mesh is utilized. For a tetrahedron element, the displacement of the four nodes is denoted by a 12×1 vector $\mathbf{u}^e = (\mathbf{u}_0{}^{\mathrm{T}}, \mathbf{u}_1{}^{\mathrm{T}}, \mathbf{u}_2{}^{\mathrm{T}}, \mathbf{u}_3{}^{\mathrm{T}})^{\mathrm{T}}$, where $\mathbf{u}_i = (u_i,\ v_i,\ w_i)^{\mathrm{T}}$. Thus the displacement field in the element can be computed by

$$\mathbf{d}(\mathbf{x}) = \sum_{i=0}^{3} N_i(\mathbf{x}) \mathbf{u}^e = \mathbf{N}\mathbf{u}^e, \quad (6)$$

where $N_i(\mathbf{x})$ are the linear shape functions, and thus $\mathbf{N}$ is a 3×12 matrix as a interpolation operator. The elastic strain energy in Equation 4 can be derived from Equations 3 and 6 as

$$U = \int_\Omega \frac{1}{2} \left(\mathbf{L}\mathbf{N}\mathbf{u}^e\right)^{\mathrm{T}} \mathbf{C} \left(\mathbf{L}\mathbf{N}\mathbf{u}^e\right) \, d\Omega. \quad (7)$$

Thus the element internal force can be derived as

$$\mathbf{f}^e_{int} = \frac{\partial U}{\partial \mathbf{u}^e} = \int_\Omega (\mathbf{L}\mathbf{N})^{\mathrm{T}} \mathbf{C} (\mathbf{L}\mathbf{N}) \, d\Omega \mathbf{u}^e = \mathbf{K}^e \mathbf{u}^e, \quad (8)$$

where $\mathbf{K}^e$ is the 12×12 element stiffness matrix, i.e.,

$$\mathbf{K}^e = (\mathbf{L}\mathbf{N})^{\mathrm{T}} \mathbf{C} (\mathbf{L}\mathbf{N}) \int_\Omega d\Omega = (\mathbf{L}\mathbf{N})^{\mathrm{T}} \mathbf{C} (\mathbf{L}\mathbf{N}) \, V^e, \quad (9)$$

and V^e is the element volume.

The linear FEM model can only be suitable for small deformations. In order to use the linear model for large deformations, we adopt the corotational model [MG04], in which the internal force $\mathbf{f}^e_{int}$ is computed by the following equation:

$$\mathbf{f}^e_{int} = \mathbf{R}^e \mathbf{K}^e \left(\left(\mathbf{R}^e\right)^{\mathrm{T}} \mathbf{x} - \mathbf{x}_0 \right), \quad (10)$$

where $\mathbf{x}$ *and* $\mathbf{x}_0$ are the deformed and undeformed position vector of the four nodes, and $\mathbf{R}^e$ is a rotation matrix, which is computed by polar decomposition of the deformation gradient. With the help of the rotational transformations, the unrealistic volume enlargement caused by large deformations can be moderated, which can approximate nonlinear deformations. As will be demonstrated in our experiments in Section 4, large deformations in the palm tree under gravity and dragging force can be performed well.

3.2. Accomodation of Fiber Field with the FEM Model

We now design the mechanism for a fiber incorporated FEM model for more physically plausible anisotropic deformations. For anisotropic materials with internal fiber structures, it is these internal fiber structures that actually control their transversely anisotropic behaviors, and our FEM model is formulated by utilizing such internal fiber orientation information.

Given the fiber orientations for the simulated object, a local frame $\{\mathbf{m}_1, \mathbf{m}_2, \mathbf{m}_3\}$ is established for each tetrahedron element: with one axis (here we use $\mathbf{m}_3$) coinciding with the fiber orientation, and the other two axes lying on the plane perpendicular to $\mathbf{m}_3$. We define a local orientation matrix as $\mathbf{M}^e = (\mathbf{m}_1, \mathbf{m}_2, \mathbf{m}_3)$, and denote quantities in this local frame by a hat '$\hat{}$'. Here, $\mathbf{M}^e$ plays an essential role in our model. Note that $\mathbf{M}^e$ is extended to a 12×12 matrix for transformation of an element.

Instead of computing the element stiffness matrix in the global frame, which is the case for isotropic materials, we compute the element stiffness matrix in local frames. The element internal force and stiffness matrix are computed by the following procedure:

1. Compute the element stiffness matrix with transversely isotropic elastic stiffness matrix $\mathbf{C}$,

$$\mathbf{K}^e = (\mathbf{L}\mathbf{N})^{\mathrm{T}} \mathbf{C} (\mathbf{L}\mathbf{N}) \, V^e.$$

2. Compute the corotated displacement vector in the local orientation frame,

$$\widehat{\mathbf{u}^e} = \mathbf{M}^e((\mathbf{R}^e)^{\mathrm{T}}\mathbf{x} - \mathbf{x}_0).$$

3. Then, the element internal force in the local frame can be computed as

$$\widehat{\mathbf{f}^e}_{int} = \mathbf{K}^e\widehat{\mathbf{u}^e}.$$

4. Thus, the element internal force in the global frame can be computed as

$$\mathbf{f}^e_{int} = \mathbf{R}^e\mathbf{M}^{e\mathrm{T}}\mathbf{K}^e\widehat{\mathbf{u}^e} = \mathbf{R}^e\widehat{\mathbf{K}^e}\left((\mathbf{R}^e)^{\mathrm{T}}\mathbf{x} - \mathbf{x}_0\right), \quad (11)$$

where $\widehat{\mathbf{K}^e} = \mathbf{M}^{e\mathrm{T}}\mathbf{K}^e\mathbf{M}^e$ is the new element stiffness matrix of our model.

By elements assembly, the matrices $\widehat{\mathbf{K}^e}$ of all the elements can be assembled to a global stiffness matrix $\widehat{\mathbf{K}}$.

Due to the fact that $\mathbf{M}^e$ can be pre-computed, $\widehat{\mathbf{K}}$ can also be pre-computed. Therefore, in our fiber incorporated model, no additional computational cost is introduced during the simulation procedure.

3.3. Implicit Time Integration for Dynamics

For the dynamics simulation, the equations of motion are then given by a system of second-order ordinary differential equations (the *Lagrangian equation*):

$$\mathbf{M}\ddot{\mathbf{u}} + \mathbf{D}\dot{\mathbf{u}} + \mathbf{f}_{int} = \mathbf{f}_{ext}. \quad (12)$$

For a tetrahedral mesh with n vertices, $\mathbf{u} \in \mathbb{R}^{3n}$, $\dot{\mathbf{u}}$ and $\ddot{\mathbf{u}}$ are the velocity and acceleration vectors. $\mathbf{M} \in \mathbb{R}^{3n\times 3n}$is the mass matrix, $\mathbf{D} \in \mathbb{R}^{3n\times 3n}$ the damping matrix, $\mathbf{f}_{int} \in \mathbb{R}^{3n}$ the internal nodal force, and $\mathbf{f}_{ext} \in \mathbb{R}^{3n}$ the external force.

An *implicit backward Euler* integration scheme [MSJT08] is used, for the reason that it is stable for large time steps. The updated (time-stepping) rule is as follows:

$$\begin{aligned} \dot{\mathbf{u}}_{t+1} &= \dot{\mathbf{u}}_t + h\ddot{\mathbf{u}}_{t+1} \\ \mathbf{u}_{t+1} &= \mathbf{u}_t + h\dot{\mathbf{u}}_{t+1} \end{aligned} \quad (13)$$

where h is the size of each time step.

At time $(t+1)$, we get

$$\dot{\mathbf{u}}_{t+1} = \dot{\mathbf{u}}_t + h\mathbf{M}^{-1}\left[\mathbf{f}_{ext} - \mathbf{D}\dot{\mathbf{u}}_{t+1} - \mathbf{R}\widehat{\mathbf{K}}\left(\mathbf{R}^{\mathrm{T}}\mathbf{x}_{t+1} - \mathbf{x}_0\right)\right]$$

$$\mathbf{x}_{t+1} = \mathbf{x}_t + h\dot{\mathbf{u}}_{t+1}$$

Finally we can get a linear system:

$$\left(\mathbf{M} + h\mathbf{D} + h^2\mathbf{R}\widehat{\mathbf{K}}\mathbf{R}^{\mathrm{T}}\right)\dot{\mathbf{u}}_{t+1} = \mathbf{M}\dot{\mathbf{u}}_t + h\left(\mathbf{f}_{ext} - \mathbf{R}\widehat{\mathbf{K}}\mathbf{R}^{\mathrm{T}}\mathbf{x}_t + \mathbf{R}\widehat{\mathbf{K}}\mathbf{x}_0\right).$$

By solving the linear system, we can get $\dot{\mathbf{u}}_{t+1}$, thus the simulation state (velocity and position vector) can be updated.

4. Experiments and Assessments

To assess the effectiveness of our algorithm, we construct several dynamic simulations with objects of transversely isotropic materials.

4.1. Impact of Fiber Field on the Elastic Stiffness

Without loss of generality, fiber orientation fields in our models are generated by a sketch-based interface. The user is allowed to draw a few strokes on the surface or a sliced internal surface boundary of the tetrahedral mesh, to roughly define the fiber directions. Then, a smooth interpolation is performed to automatically generate a smooth fiber orientation field on each nodes of the tetrahedral mesh (as in [TAI*08]). Eventually, a fiber orientation is generated for each tetrahedron element with barycentric interpolation. This procedure is illustrated with a palm tree model in Figure 1 (a) and (b). Note that the green dots represent fixed boundary nodes, the red lines are the strokes drawn by the user, and the generated elements orientation field is shown in purple.

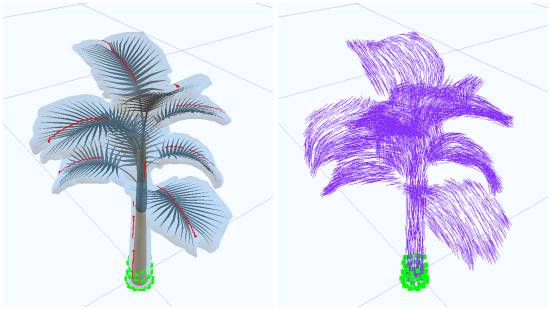

(a) drawing strokes on undeformed model (b) element fiber orientation field

Figure 1: Palm tree model: fiber field generation

As in Equation 2, five parameters can be used to define the material property of a transversely isotropic material, which affect the material's resistance to normal and shear forces. For comparison of deformation with different material properties, we start with the matrix $\mathbf{C}$ of an isotropic material such that:

$$\begin{aligned} C_{11} &= C_{22} = C_{33} = \lambda + 2\mu, \\ C_{12} &= C_{13} = C_{23} = \lambda, \\ C_{44} &= C_{55} = C_{66} = \mu, \end{aligned}$$

where λ and μ are given *Lamé coefficients* (related to Young's modulus and Poisson's ratio), and these two constants determine the constitutive model of an isotropic material. This $\mathbf{C}$ matrix can be changed according to Equation 2, and should be positive-definite. Changing C_{33} to a larger value makes the material stiffer along the fiber orientation. Likewise, other parameters can also be changed to alter the material's resistance to normal and shear forces with respect to the local frames $(\mathbf{M}^e)$.

4.2. Fibers with Heterogeneous Materials

To demonstrate the capability of our fiber incorporated FEM model, a complex palm tree model made of heterogeneous materials is simulated, i.e., the trunk and leaves have different material properties. In Figure 2, we show the deformations of the palm tree model under gravity. Figure 2 (a) shows the original undeformed model. As a basis for comparisons, Figure 2 (b) shows deformation of the whole tree which is made of an isotropic material. Being physically true, it bends to the ground if the material is too soft (inflexible to move if the material is too stiff). In Figure 2 (c), we construct the tree model using heterogeneous materials for the trunk and leaves. As can be seen, the heterogeneous FEM model gets stronger support for its trunk, preventing unnatural bending. Furthermore, in nature, a leaf is much stiffer along its vein than in the other directions, and the tree also exhibits a stiffer material property along its trunk. Based on this observation, we increase the value of C_{33}. By incorporating fibers into the heterogeneous model, we are able to achieve that, and Figure 2 (d) shows a physically plausible deformation of the palm tree. The tree now becomes stiffer along the fibers while keeping the flexible (or soft) properties in the other directions, as shown in Figure 2 (d).

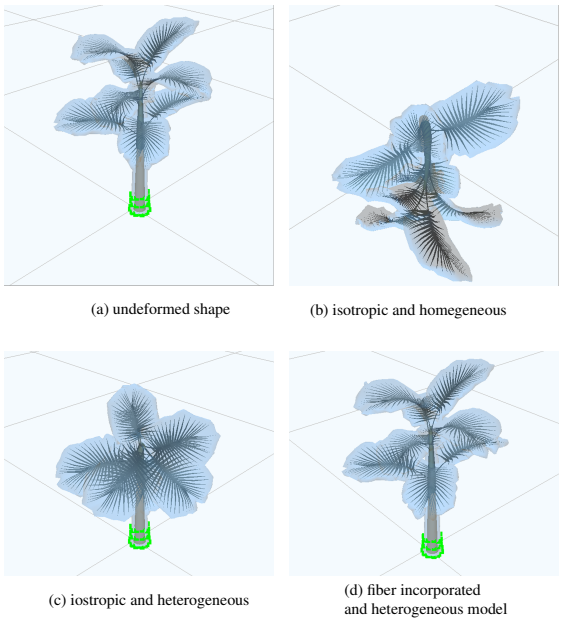

(a) undeformed shape (b) isotropic and homegeneous

(c) iostropic and heterogeneous (d) fiber incorporated and heterogeneous model

Figure 2: Comparisions of different FEM models in deformation under gravity (See the accompanying video)

Figure 3 is for the comparison of deformations of the palm tree under the same gravity and dragging force. The fiber incorporated model in Figure 3 (b) exhibits strong stiffness along the vein direction that prevents over-deformation of the trunk which is the case in Figure 3 (a). Meanwhile, the fiber model preserves the leaf from stretching as in Figure 3 (b), in contrast to the unnatural stretching of the leaf in Figure 3 (a).

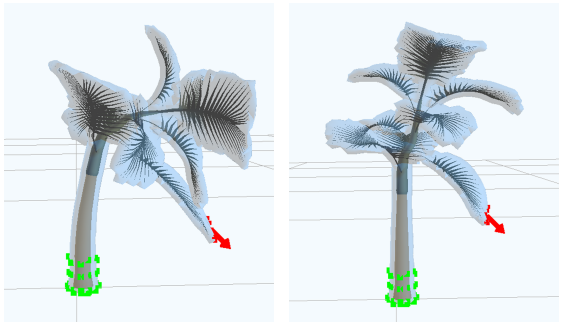

(a) without fiber (b) with fiber incorporated

Figure 3: Comparisons of deformation of the FEM models under dragging force (See the accompanying video)

Besides convincing improvement of the visual results in physically plausible deformation, the fiber incorporated FEM model only adds computational cost in precomputation, thus achieving the same performance as the existing CLFEM model. In our experiments, both the palm models with and without fibers perform at 15 fps on CPU implementation, with 5664 tetrahedrons and 2064 nodes (including 16 fixed nodes). (Intel Xeon E5507@2.27 MHz CPU, NVIDIA Quadro FX 5800 GPU.)

4.3. Fibers Incorporation with Complex Topological Structures

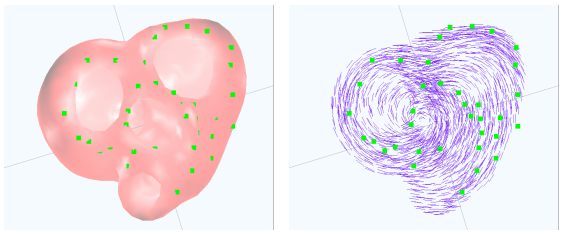

Figure 4: A beating heart simulation (See the accompanying video)

Muscular tissues are typical example of the transversely isotropic material. For example, the beating movement of the heart is controlled by the regular periodic contraction of the myocardium. Using the fiber guided model, we can simulate the complex movements of the heart beating using the given fiber orientations. To further explore the application of our fiber incorporated FEM model for more complex topological structures, we conduct an experiment with a heart which possesses two chambers and contracting muscles. The dynamic heart contraction cycles driven by periodic external forces along the fiber directions can be viewed in the accompanying video.

5. Conclusion

We have presented a fiber incorporated FEM model to deal with transversely isotropic materials, for objects with specific internal structures (heterogeneous tissues and fibers). This proposed model is proven to be effective for realistic longitudinally anisotropic deformations.

The key idea is to use a fiber orientation field to establish local element coordinate frames for FEM computation. A more flexible user interface for fiber generation and material parameters adjustment has yet to be developed. In specific applications, this orientation field can be generated even from Diffusion Tensor MRI (DTMRI) techniques (e.g. [RSG07] [SWD*09]) for more accurate mechanical and physiological analysis. This fiber FEM model can be further extended to simulate other kinds of anisotropy, such as orthotropic materials in the paper [LBKS14] that suggested using 3D *uvw* texture map to generate rotation matrix, given a local frame which can represent different material plane symmetries.

Acknowledgement We developed our C++ code based on *Vega FEM* [SSB13] by Jernej Barbič. The sketch-based interface is based on Kenshi's paper and code [TAI*08] - for non-FEM models. This work is partially supported by a research grant MOE2011-T2-2-037 (ARC 4/12) by Ministry of Education, Singapore.

References

[BJ05] BARBIČ J., JAMES D. L.: Real-time subspace integration for st. venant-kirchhoff deformable models. In *ACM Transactions on Graphics (TOG)* (2005), vol. 24, ACM, pp. 982–990. 2

[BMO*14] BENDER J., MÜLLER M., OTADUY M. A., TESCHNER M., MACKLIN M.: A survey on position-based simulation methods in computer graphics. In *Computer Graphics Forum* (2014), Wiley Online Library. 1

[CK05] CHOI M. G., KO H.-S.: Modal warping: Real-time simulation of large rotational deformation and manipulation. *Visualization and Computer Graphics, IEEE Transactions on 11*, 1 (2005), 91–101. 2

[Com10] COMAS O.: *Real-time Soft Tissue Modelling on GPU for Medical Simulation*. PhD thesis, Université des Sciences et Technologie de Lille-Lille I, 2010. 1

[ITF04] IRVING G., TERAN J., FEDKIW R.: Invertible finite elements for robust simulation of large deformation. In *Proceedings of the 2004 ACM SIGGRAPH/Eurographics symposium on Computer animation* (2004), Eurographics Association, pp. 131–140. 1

[KJ12] KIM T., JAMES D. L.: Physics-based character skinning using multidomain subspace deformations. *Visualization and Computer Graphics, IEEE Transactions on 18*, 8 (2012), 1228–1240. 2

[KTUI12] KOYAMA Y., TAKAYAMA K., UMETANI N., IGARASHI T.: Real-time example-based elastic deformation. In *Proceedings of the 11th ACM SIGGRAPH/Eurographics conference on Computer Animation* (2012), Eurographics Association, pp. 19–24. 2

[LBKS14] LI Y., BARBIC J., KOLTUN V., SIFAKIS E.: Stable orthotropic materials. In *Eurographics/ACM SIGGRAPH Symposium on Computer Animation* (2014), The Eurographics Association, pp. 41–46. 2, 6

[LHR*12] LIU N., HE X., REN Y., LI S., WANG G.: Physical material editing with structure embedding for animated solid. In *Proceedings of Graphics Interface 2012* (2012), Canadian Information Processing Society, pp. 193–200. 2

[MC11] MÜLLER M., CHENTANEZ N.: Solid simulation with oriented particles. In *ACM Transactions on Graphics (TOG)* (2011), vol. 30, ACM, p. 92. 1

[MG04] MÜLLER M., GROSS M.: Interactive virtual materials. In *Proceedings of Graphics Interface 2004* (2004), Canadian Human-Computer Communications Society, pp. 239–246. 1, 3

[MHHR07] MÜLLER M., HEIDELBERGER B., HENNIX M., RATCLIFF J.: Position based dynamics. *Journal of Visual Communication and Image Representation 18*, 2 (2007), 109–118. 1

[MHTG05] MÜLLER M., HEIDELBERGER B., TESCHNER M., GROSS M.: Meshless deformations based on shape matching. In *ACM Transactions on Graphics (TOG)* (2005), vol. 24, ACM, pp. 471–478. 1

[MJLW07] MILLER K., JOLDES G., LANCE D., WITTEK A.: Total lagrangian explicit dynamics finite element algorithm for computing soft tissue deformation. *Communications in numerical methods in engineering 23*, 2 (2007), 121–134. 1

[MSJT08] MÜLLER M., STAM J., JAMES D., THÜREY N.: Real time physics: class notes. In *ACM SIGGRAPH 2008 classes* (2008), ACM, p. 88. 4

[MTGG11] MARTIN S., THOMASZEWSKI B., GRINSPUN E., GROSS M.: Example-based elastic materials. In *ACM Transactions on Graphics (TOG)* (2011), vol. 30, ACM, p. 72. 2

[NMK*06] NEALEN A., MÜLLER M., KEISER R., BOXERMAN E., CARLSON M.: Physically based deformable models in computer graphics. In *Computer Graphics Forum* (2006), vol. 25, Wiley Online Library, pp. 809–836. 1

[RSG07] ROHMER D., SITEK A., GULLBERG G. T.: Reconstruction and visualization of fiber and laminar structure in the normal human heart from ex vivo diffusion tensor magnetic resonance imaging (dtmri) data. *Investigative radiology 42*, 11 (2007), 777–789. 6

[SSB13] SIN F. S., SCHROEDER D., BARBIČ J.: Vega: Nonlinear fem deformable object simulator. In *Computer Graphics Forum* (2013), vol. 32, Wiley Online Library, pp. 36–48. 6

[SWD*09] SOSNOVIK D. E., WANG R., DAI G., REESE T. G., WEDEEN V. J.: Diffusion mr tractography of the heart. *Journal of Cardiovascular Magnetic Resonance 11*, 1 (2009), 1–15. 6

[TAI*08] TAKAYAMA K., ASHIHARA T., IJIRI T., IGARASHI T., HARAGUCHI R., NAKAZAWA K.: A sketch-based interface for modeling myocardial fiber orientation that considers the layered structure of the ventricles. *Journal of Physiological Sciences 58*, 7 (2008), 487. 4, 6

[TH96] TING T. C., HORGAN C.: Anisotropic elasticity: theory and applications. *Journal of Applied Mechanics 63* (1996), 1056. 2

[TPBF87] TERZOPOULOS D., PLATT J., BARR A., FLEISCHER K.: Elastically deformable models. In *ACM Siggraph Computer Graphics* (1987), vol. 21, ACM, pp. 205–214. 1

[TTL12] TAN J., TURK G., LIU C. K.: Soft body locomotion. *ACM Transactions on Graphics (TOG) 31*, 4 (2012), 26. 2